

Growth and characterization of $(\text{Sc}_2\text{O}_3)_x(\text{Ga}_2\text{O}_3)_{1-x}$ by molecular beam epitaxy ^{EP}

Cite as: J. Vac. Sci. Technol. A **40**, 043403 (2022); <https://doi.org/10.1116/6.0001805>

Submitted: 17 February 2022 • Accepted: 06 May 2022 • Published Online: 24 May 2022

Mark S. Hlad, Brent P. Gila, Cammy R. Abernathy, et al.

COLLECTIONS

Paper published as part of the special topic on [Gallium Oxide Materials and Devices](#)

^{EP} This paper was selected as an Editor's Pick



View Online



Export Citation



CrossMark

ARTICLES YOU MAY BE INTERESTED IN

[A review of \$\text{Ga}_2\text{O}_3\$ materials, processing, and devices](#)

Applied Physics Reviews **5**, 011301 (2018); <https://doi.org/10.1063/1.5006941>

[A review of band structure and material properties of transparent conducting and semiconducting oxides: \$\text{Ga}_2\text{O}_3\$, \$\text{Al}_2\text{O}_3\$, \$\text{In}_2\text{O}_3\$, \$\text{ZnO}\$, \$\text{SnO}_2\$, \$\text{CdO}\$, \$\text{NiO}\$, \$\text{CuO}\$, and \$\text{Sc}_2\text{O}_3\$](#)

Applied Physics Reviews **9**, 011315 (2022); <https://doi.org/10.1063/5.0078037>

[\$\beta\$ -Gallium oxide power electronics](#)

APL Materials **10**, 029201 (2022); <https://doi.org/10.1063/5.0060327>



HIDEN
ANALYTICAL



Instruments for Advanced Science

- Knowledge,
- Experience,
- Expertise

Click to view our product catalogue

Contact Hiden Analytical for further details:
www.HidenAnalytical.com
info@hideninc.com



Gas Analysis

- ▶ dynamic measurement of reaction gas streams
- ▶ catalysis and thermal analysis
- ▶ molecular beam studies
- ▶ dissolved species probes
- ▶ fermentation, environmental and ecological studies



Surface Science

- ▶ UHVTPD
- ▶ SIMS
- ▶ end point detection in ion beam etch
- ▶ elemental imaging - surface mapping



Plasma Diagnostics

- ▶ plasma source characterization
- ▶ etch and deposition process reaction kinetic studies
- ▶ analysis of neutral and radical species



Vacuum Analysis

- ▶ partial pressure measurement and control of process gases
- ▶ reactive sputter process control
- ▶ vacuum diagnostics
- ▶ vacuum coating process monitoring

Growth and characterization of $(\text{Sc}_2\text{O}_3)_x(\text{Ga}_2\text{O}_3)_{1-x}$ by molecular beam epitaxy

Cite as: J. Vac. Sci. Technol. A 40, 043403 (2022); doi: 10.1116/6.0001805

Submitted: 17 February 2022 · Accepted: 6 May 2022 ·

Published Online: 24 May 2022



Mark S. Hlad,^{1,a)} Brent P. Gila,¹ Cammy R. Abernathy,¹ Fan Ren,²  and S. J. Pearton^{1,b)} 

AFFILIATIONS

¹Department of Materials Science and Engineering, University of Florida, Gainesville, Florida 32611

²Department of Chemical Engineering, University of Florida, Gainesville, Florida 32611

Note: This paper is part of the Special Topic Collection on Gallium Oxide Materials and Devices.

a)Electronic mail: spear@mse.ufl.edu

b)Permanent address: Intel, 5000 W Chandler Blvd, Chandler, AZ 8522

ABSTRACT

$(\text{Sc}_2\text{O}_3)_x(\text{Ga}_2\text{O}_3)_{1-x}$ was grown by molecular beam epitaxy at low temperatures (100 °C) using a variety of growth sequences to avoid surface segregation of Ga. Continuous and digital growth techniques always produced Ga segregation. This surface segregation was attributed to the stronger bond between the Sc and O compared to the Ga and O. A digital growth technique (alternate opening of Sc and Ga shutters with the O shutter open continuously during the growth) was unsuccessful in eliminating this effect. The segregation was eliminated using a growth technique in which the Ga shutter was closed for a set amount of time toward the end of the growth while the O and Sc shutters remained open. Characterization with reflection high energy electron diffraction, x-ray diffraction, and transmission electron microscopy revealed the growth of a fine-grained polycrystalline film under these conditions. A third growth technique was used that involved closing the Ga shutter for a set amount of time toward the end of the growth while the O and Sc shutters were open continuously. This technique was successful in depositing a uniform film. However, the breakdown field was only 1.40 MV/cm (at 1 mA/cm²). The addition of Ga to Sc_2O_3 diminished the insulating properties of the film. These initial experiments indicate that phase segregation is likely to be a major issue with most growth techniques and that alloying Ga_2O_3 with elements other than Sc, such as Gd or Al, might be a more successful approach.

Published under an exclusive license by the AVS. <https://doi.org/10.1116/6.0001805>

I. INTRODUCTION

There is significant current interest in developing ultrawide bandgap alloys for use as dielectrics or active regions in power electronics, UV photodetectors, and transparent coatings.^{1–5} There are a number of systems under investigation, including β - $(\text{Al}_x\text{Ga}_{1-x})_2\text{O}_3$,^{6,7} which has issues with phase segregation at moderate Al compositions; $(\text{Mg}_x\text{Ga}_{1-x})_2\text{O}_3$ alloys, which also have issues due to the cubic rock salt symmetry of MgO limiting solubility with monoclinic Ga_2O_3 ;⁸ $(\text{B}_x\text{Ga}_{1-x})_2\text{O}_3$ alloys;⁹ and finally $(\text{Sc}_x\text{Al}_{1-x})\text{N}$.^{10,11} The latter is attracting attention for acoustoelectric and ferroelectric applications and high channel charge density ScAlN/GaN high electron mobility transistors.^{12–19}

One system that has not been investigated in detail is $(\text{Sc}_2\text{O}_3)_x(\text{Ga}_2\text{O}_3)_{1-x}$. A specific application for this would be as an amorphous film in a stacked gate dielectric with a crystalline oxide

on materials like GaN.^{20,21} For example, previous trends have shown that the smaller the lattice mismatch to GaN, the smaller the interface state density.²² However, dislocation defects in the crystalline oxide (due to the lattice mismatch with GaN) act as current leakage paths that limit the breakdown voltage. Depositing an amorphous dielectric on top of the crystalline oxide would allow the properties of the oxide/GaN interface to be maintained while reducing the current leakage by terminating dislocation defects in the crystalline oxide. Previous results of a stacked gate dielectric with SiO_2 deposited on top of Gd_2O_3 showed improvement of the breakdown field from 0.3 to 0.8 MV/cm.^{22–24}

Bixbyite Sc_2O_3 has a large bandgap (6.3 eV) and high dielectric constant of 14 and when alloyed with Ga_2O_3 could provide a significant bandgap span,^{20,22,24} which depends on the crystal symmetry that was stable at a particular set of growth conditions and Sc contents.²² For example, monoclinic β - Ga_2O_3 has a bandgap of

~4.8 eV and hexagonal α -polytype Ga_2O_3 has a bandgap of ~5.1 eV.^{1,2} The crystal structures of monoclinic and hexagonal Sc_2O_3 phases are similar to those of β - and α - Ga_2O_3 , respectively. Zhu *et al.*¹⁹ have recently reported density functional calculations of the structural and electronic properties of $(\text{Sc}_x\text{Ga}_{1-x})_2\text{O}_3$ alloys and found that they preferentially form in the hexagonal phase with negative formation enthalpies, rather than monoclinic phases with positive formation enthalpies. There has been limited effort on growth of $(\text{Sc}_2\text{O}_3)_x(\text{Ga}_2\text{O}_3)_{1-x}$. In this paper, we report initial investigations into the synthesis of such films and methods to avoid Ga surface segregation.

II. EXPERIMENT

A Riber 2300 MBE system was used for all growths.^{20,24} The growth chamber was pumped down to $1\text{--}5 \times 10^{-9}$ Torr using an Oxford Cryo-Torr 8 cryopump. The MBE system is equipped with a reflective high energy electron diffraction (RHEED) gun to provide *in situ* characterization of the oxide film during growth. The MBE system contains six ports with five of them containing Knudsen cells (3 Riber 125 IK's with 25 cc crucibles, 1 Varian 0981-4135 with a 40 cc crucible, and 1 EPI 91-734 with a 25 cc crucible) for various sources (Sc, Ga, Mg, Ca, and Sm) and the remaining port containing the oxygen plasma source. The temperature of the Knudsen cells is controlled by a FICS 10 controller that adjusts the power output of an external power supply whose power cables are connected to two posts on the cell.

An MDP21 radio frequency source from Oxford Applied Research was used as the oxygen source and operated at 13.56 MHz with a forward power of 300 W and a reflected power of 2–3 W. Oxygen (99.995%) was supplied to the plasma head using a high purity 8161c Unit (Celerity) O_2 mass flow controller that had a 3 SCCM full scale range. The substrate temperature was measured using a backside thermocouple in close proximity to the substrate holder. The substrate thermocouple was calibrated by using pieces of GaSb and InSb, which have melting points of 707 and 525 °C respectively.

All substrates received an *ex situ* and *in situ* surface treatment prior to oxide deposition to remove any surface contamination. Prior to treating the surfaces, the substrates were inspected under a microscope, and an RMS roughness was determined by AFM as a reference value. The substrates used for oxide deposition included 50 mm diameter (100), P-doped (n-type) Si substrates from Wacker-Chemitronic GMBH. Each Si wafer was soaked in buffered oxide etch (BOE) solution (6:1 $\text{NH}_4\text{F}:\text{HF}$ in water) to remove the native oxide layer, followed by rinsing in de-ionized water and blow drying with filtered N_2 . An RMS surface roughness value of 0.08 nm was measured with AFM following this surface treatment. They were then immediately indium mounted to a molybdenum block and then placed under vacuum inside the load lock of the MBE system. The samples were then cleaned *in situ* by heating to 200 °C to drive off any moisture that collected on the surface between the time it was etched in BOE and placed under vacuum.

We also used GaN wafers grown by MOCVD. These had a surface roughness of 0.13 nm RMS using a $1\ \mu\text{m}$ scan. Each GaN sample received an *ex situ* treatment starting with a 3 min HCl: H_2O (1:1) solution to degrease the sample and remove oxygen and

carbon contamination. This was followed by rinsing in de-ionized water and then drying with filtered N_2 , followed by a 25 min UV- O_3 treatment in a UVOCS UVO cleaner (model number 42-220) to remove residual carbon. The sample was finally placed in a 5 min BOE solution to remove the native oxide formed from the UV- O_3 treatment and then rinsed in de-ionized water and dried with N_2 . Successful removal of the native oxide was observed with RHEED images of the surface. The RHEED pattern of the surface with the native oxide showed arcs, and the RHEED pattern of the BOE treated surface showed streaks.

After receiving *ex situ* treatment, GaN was immediately indium mounted to an Mo block and then placed under vacuum inside the load lock of the MBE system. The sample was then given an *in situ* thermal treatment at 700 °C for 10 min to remove any oxygen or carbon contamination on the surface that was not removed during the *ex situ* treatments. The room temperature RHEED pattern showed a (1×1) surface and a (1×3) pattern appeared after the *in situ* thermal treatment at 700 °C.

Scandium gallium oxide films were deposited using a 99.999% pure Sc rod and 99.9999% pure Ga ingot. The Sc Knudsen cell temperatures ranged from 1170 to 1200 °C and the Ga Knudsen cell temperatures ranged from 700 to 884 °C. A substrate temperature of 100 °C was used with an oxygen pressure ranging from 8×10^{-6} to 1.1×10^{-5} Torr with an Oxford RF plasma source at 300 W forward power and 2–3 W reflective power. Sample rotation was kept constant at 15 rpm during the film growth. Numerous growth techniques were employed to grow a continuous film with good electrical properties. The films were generally grown under O-rich conditions using a meta/oxygen ratio of <1. The Sc flux (in the range of a few nA) was calibrated using a quartz crystal monitor inserted below the substrate before growth, and nominally constant Sc flux was maintained during growth. Calibration samples were used to measure Sc concentration and layer thickness using Auger electron spectroscopy (AES), x-ray photoemission spectroscopy (XPS), and x-ray diffraction (XRD).

An FIB FEI Strata DB (dual beam) 235 was used to prepare the oxide films, and a TEM 2010F operating at 400 keV was used for high-resolution analysis of the crystal structure of the oxide films. A Philips APD 3720 x-ray powder diffractometer was used to characterize the oxide films. Samples were analyzed using a $\text{Cu K}\alpha$ x-ray source, and a 2θ range of 20°–85° was scanned using 0.02° increments. Crystal phases were identified by standards taken from the JCPDS Powder Diffraction File. All identified peaks were calibrated to the GaN (004) peak position ($2\theta = 73.078^\circ$). A Phillips MPD 1880/HR with a five-crystal analyzer and $\text{Cu K}\alpha$ x-ray source was used for x-ray reflectivity measurements. Measurements included film thickness and interfacial roughness. A Perkin-Elmer PHI 5100 ESCA system was used for all XPS and a Perkin-Elmer PHI 660 Scanning Auger Multiprobe was used for AES characterization.

After the oxide films were deposited and the samples removed from the MBE system and molybdenum block, they were processed to make MOS capacitors.²⁴ The first processing step involved opening up ohmic windows so that the exposed oxide could be etched away. The second step was deposition of ohmic contacts in the areas of oxide that were etched away. A thin ring of GaN between the oxide island and the ohmic contact was left open so that the oxide could be electrically isolated from the ohmic pad.

The final processing step involved depositing metal gates of 50 or 100 μm in diameter on top of the oxide island. Fabrication of the MOS capacitors allowed current-voltage (I - V) measurements to be taken, which helped determine the performance of the oxide. A

Hewlett Packard Model 4145 was used to make I - V measurements, with the current compliance set at 100 nA. The voltage was swept in both negative and positive directions until the forward and reverse breakdowns were reached. Voltages were extracted from the I - V plot at 19.6 nA for diodes with 50 μm gates and at 78.5 nA for diodes with 100 μm gates. A Hewlett Packard Model 4284 LCR connected to a LAB VIEW based PC was used to make capacitance-voltage measurements.

III. RESULTS AND DISCUSSION

A. Continuous growth of $(\text{Sc}_2\text{O}_3)_x(\text{Ga}_2\text{O}_3)_{1-x}$

The use of both Sc and Ga in the oxide films served two purposes. Since previous Sc_2O_3 films deposited at 100 $^\circ\text{C}$ using a high Sc flux were polycrystalline, it was hoped that adding Ga would frustrate the Sc_2O_3 lattice and promote amorphous film growth. This would be desirable for films used as dielectrics. The second purpose was using Sc to stabilize Ga in the 3⁺ oxidation state. While Sc has a single oxidation state of 3⁺, Ga has multiple

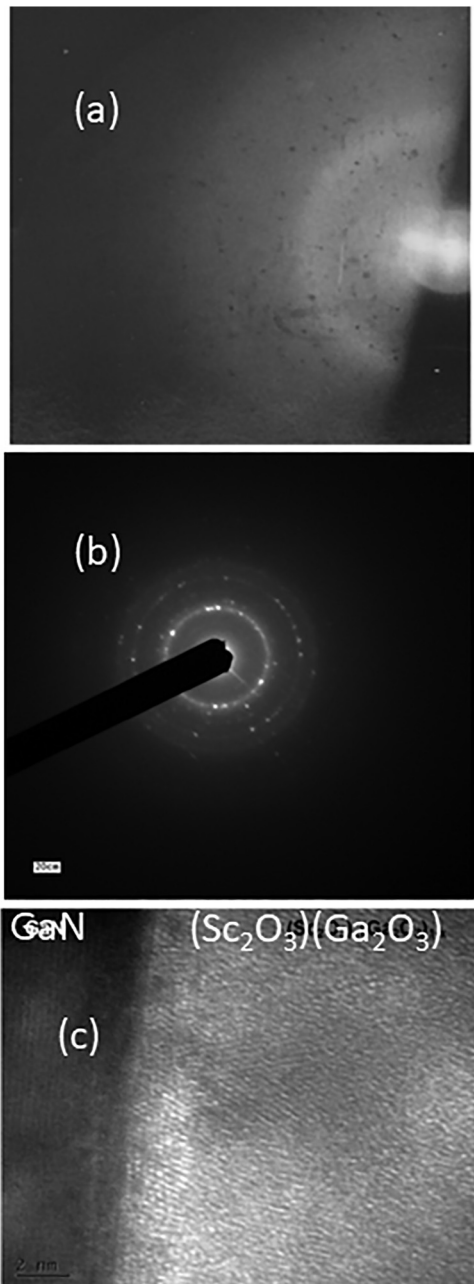


FIG. 1. (a) RHEED image of $(\text{Sc}_2\text{O}_3)_x(\text{Ga}_2\text{O}_3)_{1-x}$ on GaN during and after growth. (b) TEM SAD pattern of $(\text{Sc}_2\text{O}_3)_x(\text{Ga}_2\text{O}_3)_{1-x}$ on GaN. (c) HRTEM image of $(\text{Sc}_2\text{O}_3)_x(\text{Ga}_2\text{O}_3)_{1-x}$ on GaN.

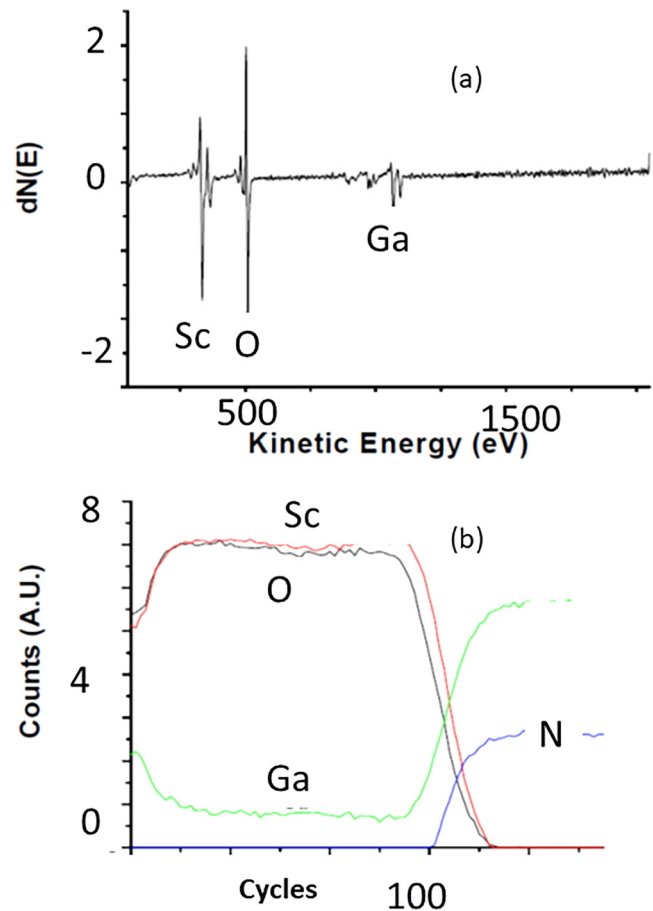


FIG. 2. AES analysis of continuous growth for $(\text{Sc}_2\text{O}_3)_x(\text{Ga}_2\text{O}_3)_{1-x}$ on GaN. (a) Surface scan. (b) Depth profile.

oxidation states of 3^+ , 2^+ , and 1^+ . It is believed that the addition of an electropositive element in a ternary phase will stabilize the higher oxidation state for a metal with multiple oxidation states (examples include KMnO_4 , SrFeO_4 and BaPbO_3).^{25,26}

Low substrate temperatures and high growth rates are typically used to foster amorphous film growth in MBE. Therefore, a substrate temperature of 100°C was used, and cell temperatures of 1190°C (corresponding to a Sc_2O_3 growth rate of 3.2 nm/min) and 884°C (corresponding to a Ga_2O_3 growth rate of 2.3 nm/min) were used for Sc and Ga, respectively. The RF oxygen plasma was set at a pressure of $8.0 \times 10^{-6}\text{ Torr}$ with a forward power of 300 W . A continuous growth was used in which all three shutters were simultaneously open during the growth. During the growth and at the end of the growth, RHEED showed a light arc, as shown in Fig. 1(a) and indicative of polycrystalline film growth. TEM also showed arcs in the Selected Area Diffraction (SAD) pattern, Fig. 1(b), while an HRTEM image in Fig. 1(c) shows the rotation of grains in different directions. Analysis with XRD revealed no peaks (except for those of the GaN and sapphire), providing further evidence that a fine-grained polycrystalline film was present with no preferred orientation. Characterization with AFM showed an RMS roughness of 5.65 nm for a $1\mu\text{m}$ scan and an RMS roughness of 6.78 nm for a $5\mu\text{m}$ scan. The high surface roughness was associated with the extremely high growth rate of 6.0 nm/min .

An AES surface scan revealed that the films were rich in Sc, with an Sc to Ga peak-to-peak ratio of 2.25, as shown in Fig. 2(a). A depth profile revealed surface segregation of Ga, Fig. 2(b). One of the mechanisms that drive surface enrichment is the segregation of the species with the weakest bond.²⁷ The segregation of Ga was attributed to the weaker bond between Ga and O compared to Sc and O. Looking at the electronegativity values for Sc (1.2) and Ga (1.82), Sc is much more electropositive than Ga and has a higher reactivity in forming a compound with O (3.44).²⁸ Segregation is generally eliminated by growing in a kinetically limited regime at low temperatures and high growth rates.^{29–31} Since the surface

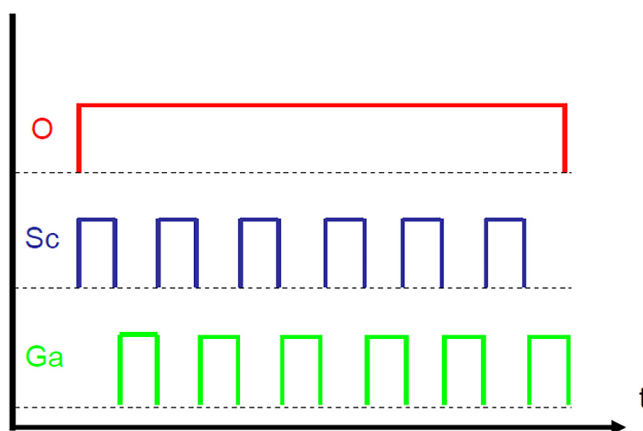


FIG. 3. Diagram of a digital growth technique in which the Sc and Ga shutters are alternated for a given time sequence while the oxygen shutter is open continuously throughout the entire growth.

enrichment of Ga in $(\text{Sc}_2\text{O}_3)_x(\text{Ga}_2\text{O}_3)_{1-x}$ occurred under these growth conditions, alternative growth techniques were investigated to eliminate the Ga segregation.

B. Digital growth of $(\text{Sc}_2\text{O}_3)_x(\text{Ga}_2\text{O}_3)_{1-x}$

In an attempt to eliminate the segregation of Ga at the surface, a digital growth technique was used. This technique was previously used for MgCaO to prevent the segregation of Ca.³² The

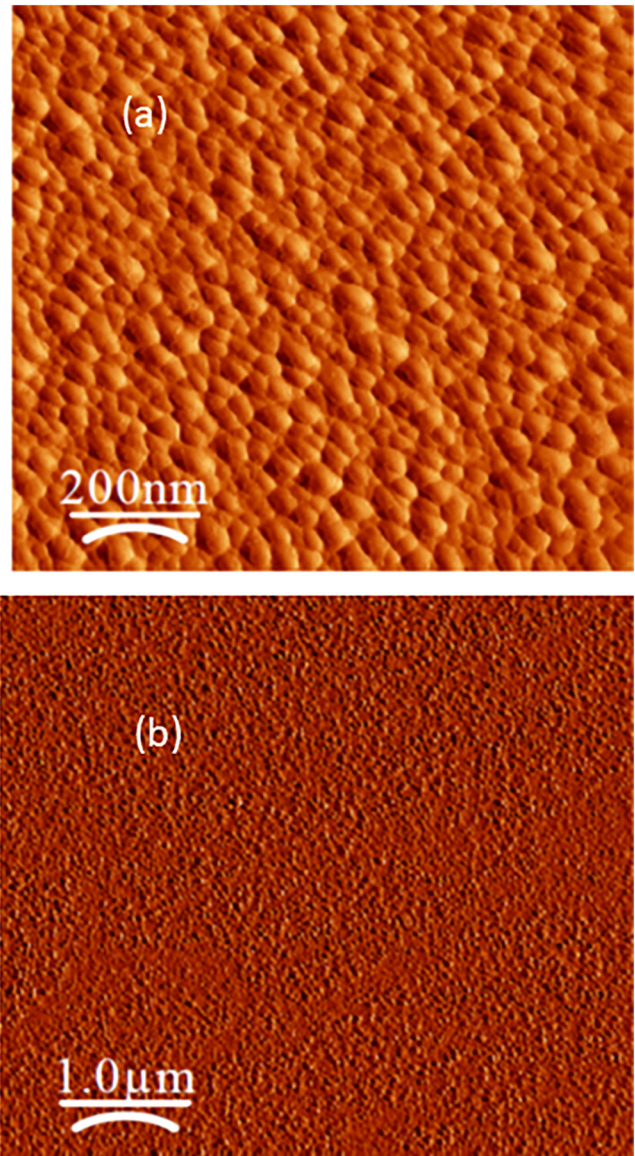


FIG. 4. AFM images of $(\text{Sc}_2\text{O}_3)_x(\text{Ga}_2\text{O}_3)_{1-x}$ on GaN for a digital growth. (a) $1\mu\text{m}$ scan with RMS roughness of 4.12 nm . (b) $5\mu\text{m}$ scan with RMS roughness of 5.01 nm .

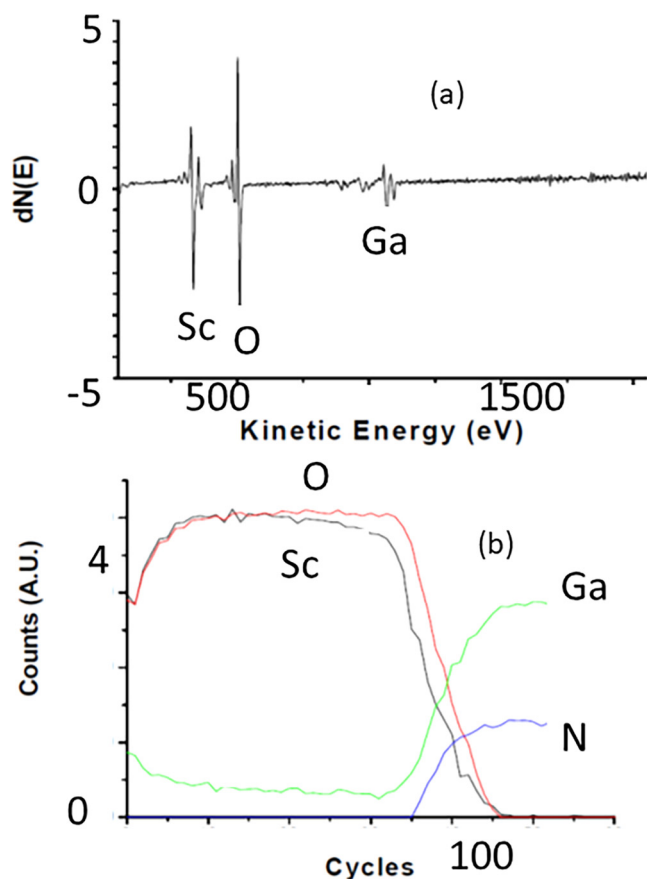


FIG. 5. AES analysis of digital growth for $(Sc_2O_3)_x(Ga_2O_3)_{1-x}$ on GaN. (a) Surface scan. (b) Depth profile.

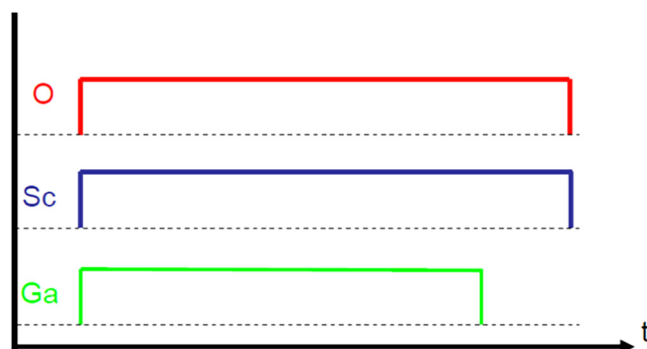


FIG. 6. Diagram of growth technique in which the Ga shutter is closed toward the end of the growth for a designated amount of time while the Sc and O shutters are open continuously.

TABLE I. Auger peak-to-peak ratios for Ga:O, Sc:O, and Sc:Ga as function of the amount of time that the Ga shutter was closed toward the end of the growth.

Ga shutter closure time(s)	Ga:O	Sc:O	Sc:Ga
0	0.21	0.48	2.25
30	0.18	0.54	3.10
45	0.14	0.56	3.90
60	0.11	0.59	4.44
75	0.11	0.60	5.38
90	0.11	0.61	5.66
120	0.08	0.65	7.96

digital growth involved repeatedly alternating the opening and closing of the Sc and Ga shutters at 10 s intervals (10:10) during continuous exposure from the oxygen plasma, as shown in Fig. 3. A polycrystalline RHEED pattern was present for the entire growth,

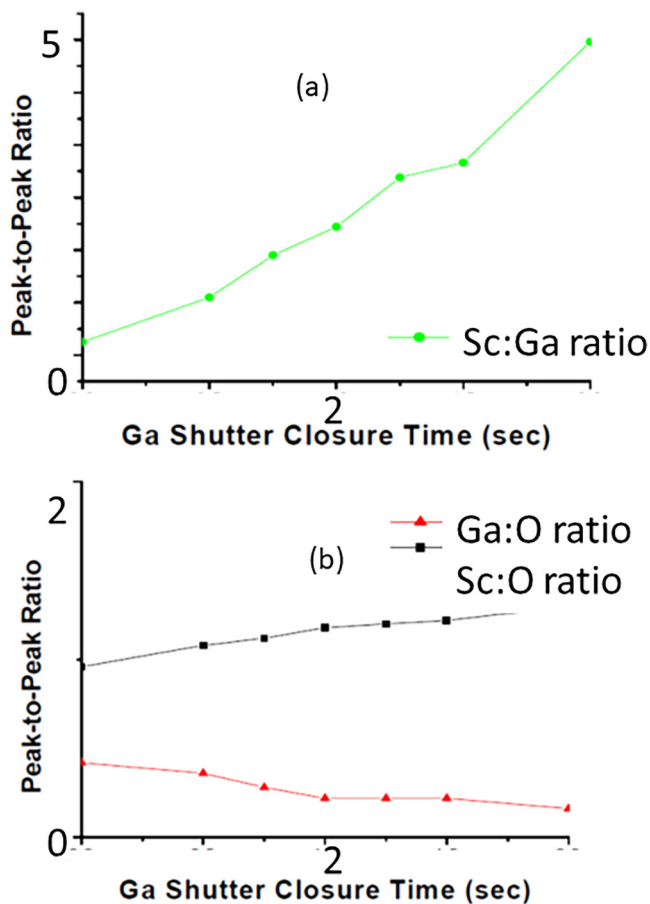


FIG. 7. Change in Auger peak-to-peak ratios as a function of the amount of time that the Ga shutter is closed toward the end of growth. (a) Sc:Ga. (b) Ga:O and Sc:O.

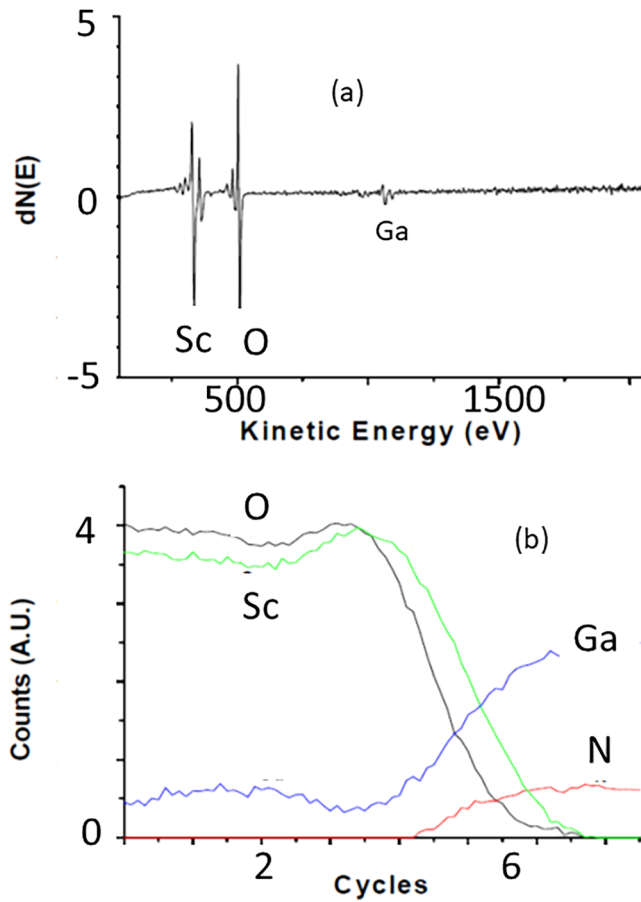


FIG. 8. AES analysis of growth with Ga shutter closure for $(\text{Sc}_2\text{O}_3)_x(\text{Ga}_2\text{O}_3)_{1-x}$ on GaN. (a) Surface scan. (b) Depth profile.

and no peaks appeared in the XRD scan except for peaks from the substrate. AFM showed an RMS roughness of 4.12 nm for a $1\ \mu\text{m}$ scan and an RMS roughness of 5.01 nm for a $5\ \mu\text{m}$ scan as shown in Fig. 4. The surface roughness was lower compared to the surface roughness for the continuous growth. This was attributed to the lower growth rate of 3.0 nm/min compared to the 5.5 nm/min growth rate for the continuous growth. The AES depth profile in Fig. 5 shows that the digital growth technique did not eliminate the segregation of Ga at the surface of the films.

We did not change the O pressure for techniques A and B, but this is not expected to overcome the poor-quality growth observed.

C. Growth with closure of Ga shutter

A third growth technique employed involved closing the Ga shutter toward the end of the growth for a certain amount of time while the Sc and O shutters remained open continuously, as shown in Fig. 6. This technique was previously employed to eliminate the segregation of In in the growth of InGaN.³³ The oxygen pressure

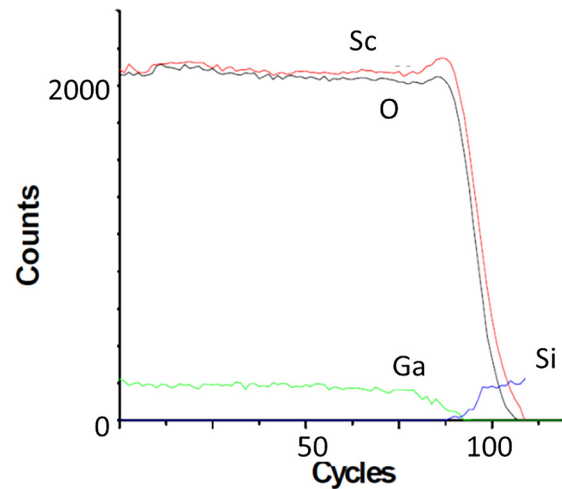


FIG. 9. AES depth profile of growth with Ga shutter closure for $(\text{Sc}_2\text{O}_3)_x(\text{Ga}_2\text{O}_3)_{1-x}$ on Si.

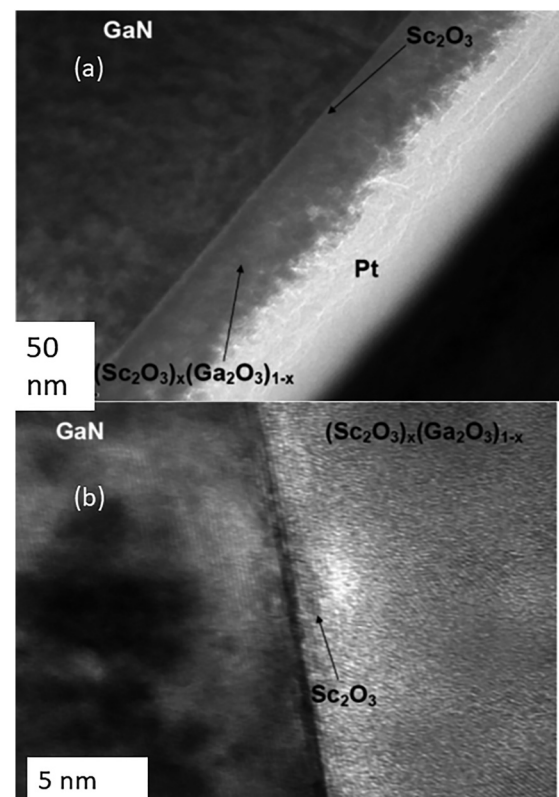


FIG. 10. (a) Low magnification cross-sectional TEM image of $(\text{Sc}_2\text{O}_3)_x(\text{Ga}_2\text{O}_3)_{1-x}$ on GaN with a thin Sc_2O_3 layer at the GaN/oxide interface. (b) High magnification cross-sectional TEM image of $(\text{Sc}_2\text{O}_3)_x(\text{Ga}_2\text{O}_3)_{1-x}$ on GaN with a thin Sc_2O_3 layer at the GaN/oxide interface.

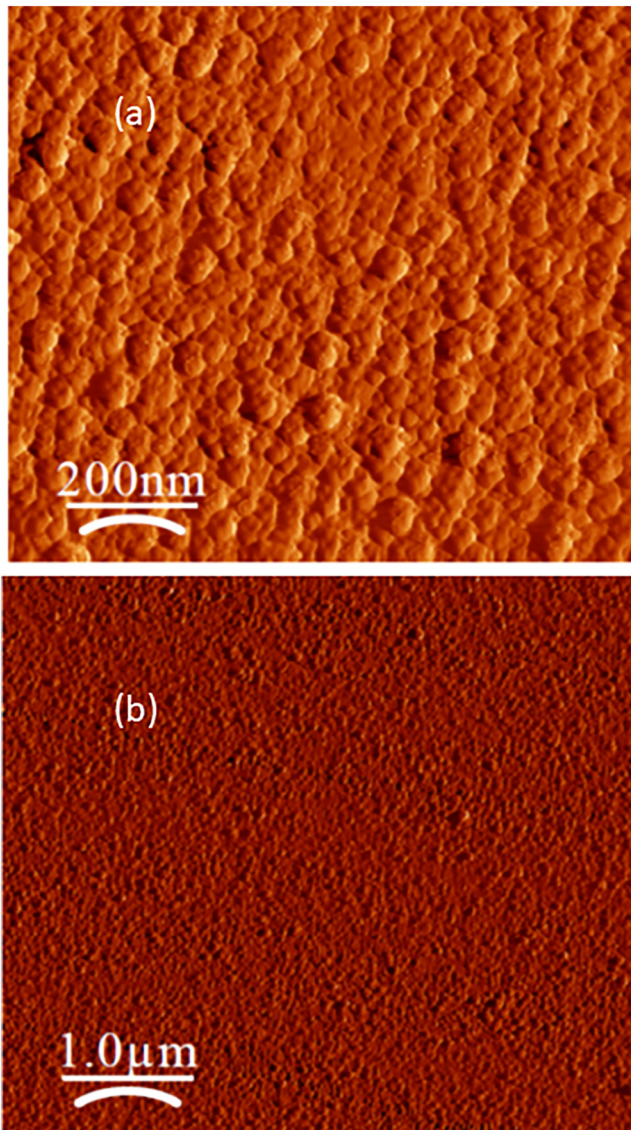


FIG. 11. AFM images of $(\text{Sc}_2\text{O}_3)_x(\text{Ga}_2\text{O}_3)_{1-x}$ on GaN for a growth with the Ga shutter closed toward the end. (a) $1\ \mu\text{m}$ scan with RMS roughness of 2.98 nm. (b) $5\ \mu\text{m}$ scan with RMS roughness of 3.79 nm.

was also increased to 1.2×10^{-5} Torr to increase the VI/III ratio. Various conditions were investigated to determine the optimal parameters to eliminate the surface enrichment of Ga. Table I and Fig. 7 show that the Sc:O and Sc:Ga ratios increase with increasing time that the Ga shutter was closed toward the end of the growth, and the Ga:O ratio decreases with increasing time. The composition of the films was $(\text{Sc}_2\text{O}_3)_{0.68}(\text{Ga}_2\text{O}_3)_{0.32}$ for 0 s shutter closure and $(\text{Sc}_2\text{O}_3)_{0.86}(\text{Ga}_2\text{O}_3)_{0.14}$ for 120 s closure. It was determined that closing the Ga shutter for the final 90 s of a 6 min growth successfully eliminated the segregation of Ga, as shown in Fig. 8.

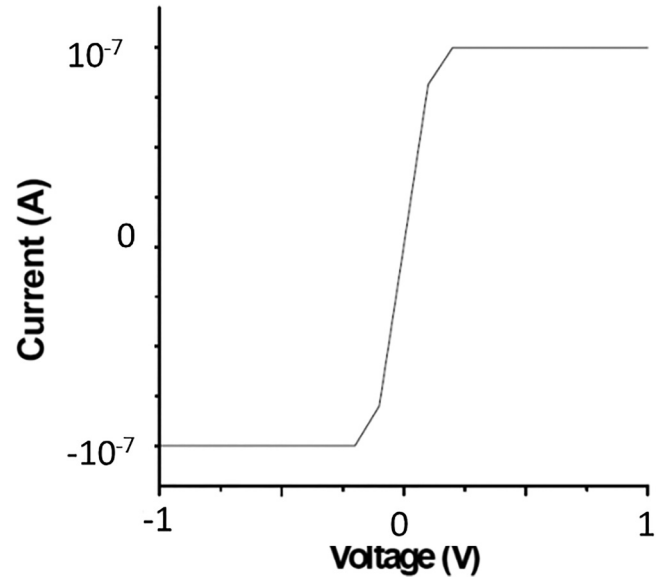


FIG. 12. I - V plot of $(\text{Sc}_2\text{O}_3)_x(\text{Ga}_2\text{O}_3)_{1-x}$ film deposited at $100\ ^\circ\text{C}$. Film stoichiometry was rich in Sc.

In the depth profile, the intensities of the Sc and O increase and the intensity of the Ga decreases at the oxide/GaN interface. This same effect was also present in samples with $(\text{Sc}_2\text{O}_3)_x(\text{Ga}_2\text{O}_3)_{1-x}$ on Si, as shown in Fig. 9. Further analysis with HRTEM showed a thin, faint line at the interface, as shown in Fig. 10(a). This was also seen in an HRTEM cross-sectional image of $(\text{Ga}_2\text{O}_3)_x(\text{Gd}_2\text{O}_3)_{1-x}$ on GaAs.³⁴ The thin layer on GaAs (2–3 monolayers) was identified as single crystal Gd_2O_3 . The initial formation of a Gd_2O_3 layer was attributed to Gd (electronegativity of 1.2) having a higher reactivity with oxygen and being more electropositive compared to Ga (electronegativity of 1.82). Since Sc has the same electronegativity value as Gd and has a much greater value than Ga, it appears that a similar trend is present in the $(\text{Sc}_2\text{O}_3)_x(\text{Ga}_2\text{O}_3)_{1-x}$ film with the thin layer at the interface representing Sc_2O_3 , as shown in Fig. 10(b). Characterization with AFM showed a RMS roughness of 2.98 nm for

TABLE II. Characteristic binding energies of possible phases present in $(\text{Sc}_2\text{O}_3)_x(\text{Ga}_2\text{O}_3)_{1-x}$.

Element	Spectral line	Phase	Binding energy (eV)
Ga	LMM (Auger)	Ga_2O_3	191.2
Ga	LMM (Auger)	Ga	185.3
Ga	$2p_{3/2}$	Ga_2O_3	20.5
Ga	$2p_{3/2}$	Ga	18.5
Ga	3d	Ga_2O_3	1117.8
Ga	3d	Ga	1116.5
Sc	$2p_{3/2}$	Sc_2O_3	401.9
Sc	$2p_{3/2}$	Sc	398.3

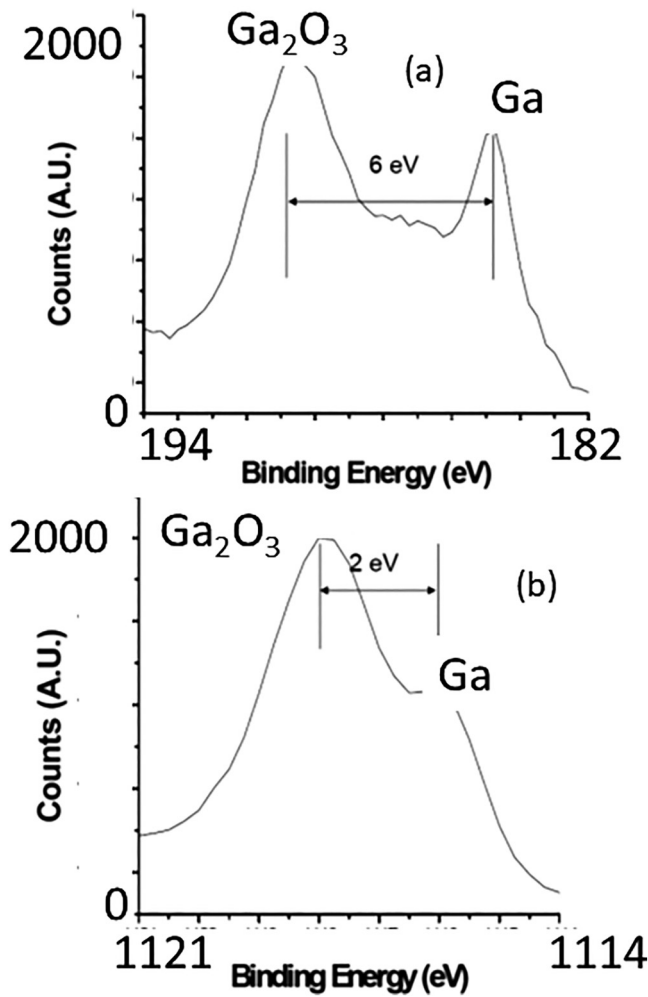


FIG. 13. (a) Ga LMM level shows a 6 eV difference between the Ga₂O₃ and Ga metal peaks. (b) Ga 2p_{3/2} level shows a 2 eV difference between the Ga₂O₃ and Ga metal peaks.

a 1 μm scan and an RMS roughness of 3.79 nm for a 5 μm scan, as shown in Fig. 11. The high surface roughness was a result of the high 5.5 nm/min growth rate. However, the surface roughness was lower compared to the surface roughness for the continuous and digital growths. This was attributed to the elimination of the Ga surface segregation.³⁵

It is important to note that in this last approach, we eliminated Ga segregation by closing the Ga shutter before the end of growth but also increased the O pressure, as compared to continuous or digital growth. An increase in O flux, however, may also kinetically favor the incorporation of Ga into (Sc₂O₃)_x(Ga₂O₃)_{1-x}, i.e., may reduce Ga segregation. Of these two effects, closing the Ga shutter before the end of growth and increasing the O flux, the former was much more important in reducing Ga segregation.

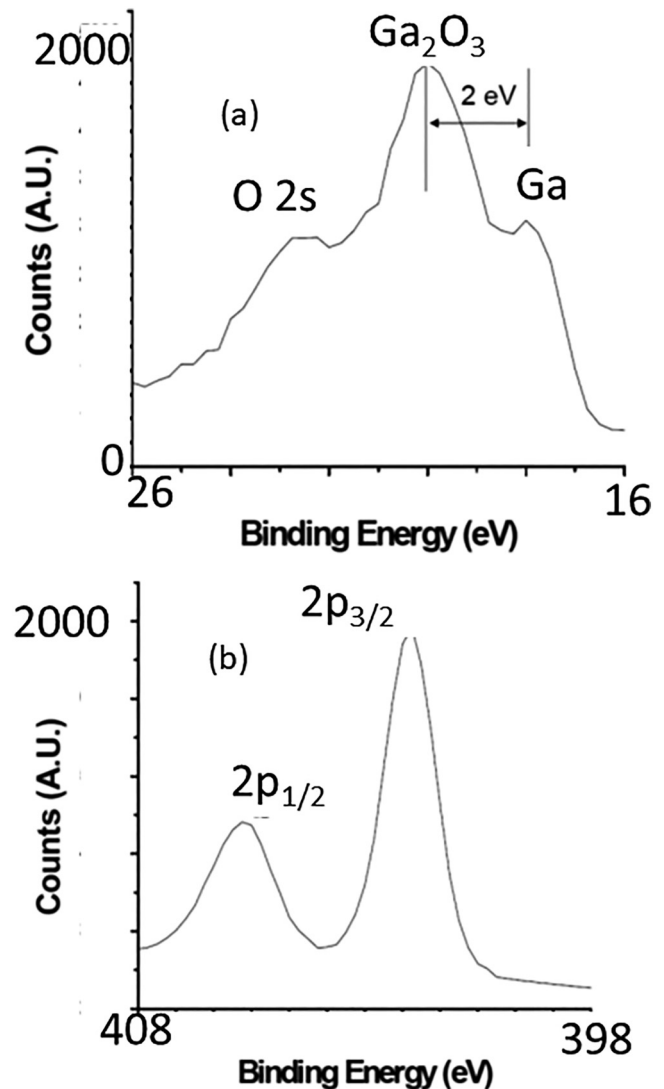


FIG. 14. (a) Ga 3d level shows a 2 eV difference between the Ga₂O₃ and Ga metal peaks. (b) Sc 2p_{3/2} level only shows the presence of a Sc₂O₃ phase.

TABLE III. Breakdown voltage as a function of decreasing Ga cell temperature.

Sample	T _{Ga} (°C)	T _{Sc} (°C)	t _{ox} (nm)	G (nm/min)	V _{bd} (MV/cm) at 1 mA/cm ²
1	865	1190	33	5.5	0.15
2	770	1180	47	2.4	0.70
3	750	1180	42	2.1	1.00
4	725	1180	40	2.0	1.40

D. Electrical testing of $(\text{Sc}_2\text{O}_3)_x(\text{Ga}_2\text{O}_3)_{1-x}$

After fabricating MOS capacitors, I - V measurements were taken to determine the breakdown voltage. Figure 12 shows that the $(\text{Sc}_2\text{O}_3)_x(\text{Ga}_2\text{O}_3)_{1-x}$ film (33 nm) has a poor breakdown field of 0.15 MV/cm at 1 mA/cm². The leakage current is so high that the oxide appears to be more of a conductor. The low breakdown field is indicative of a mode A failure due to defects or pinholes in the oxide or defects at the oxide/semiconductor interface. The film was analyzed further with XPS to determine the root cause of this premature breakdown. The National Institute of Standards and Technology (NIST) XPS database³⁶ was used to reference the characteristic binding energies of all the possible chemical species present in the $(\text{Sc}_2\text{O}_3)_x(\text{Ga}_2\text{O}_3)_{1-x}$ film (Table II). The objective of the XPS analysis was to determine if free Ga or Sc metal was present in the film that could create an electrical pathway between the metal gate and GaN substrate. Figures 13 and 14 indicate the presence of both Ga_2O_3 and Ga metal phases. A 6 eV difference between the two phases is seen for the Ga LMM (L-inner level-M-inner level-M-inner level electron transition) (Auger) energy level, and a 2 eV difference between the two phases is seen for both the Ga 2p_{3/2} and 3d energy levels. Analysis of the Sc 2p_{3/2} energy level revealed that only the Sc_2O_3 phase is present. A peak at 401.9 eV corresponding to Sc_2O_3 is present, but no peak appears at 398.3 eV, which is indicative of Sc metal. It can be seen from the XPS data that the free Ga metal present in the film was responsible for the poor breakdown field.

After determining the root cause of the breakdown, $(\text{Sc}_2\text{O}_3)_x(\text{Ga}_2\text{O}_3)_{1-x}$ films were grown at lower Ga cell temperatures to eliminate the free Ga metal present in the oxide. The Sc cell temperature was also reduced to make more O atoms available to the Ga atoms and to reduce the overall metal to oxygen ratio, which was higher than desired. Table III shows the breakdown voltage increases as the Ga cell temperature decreases, but were still poor. Below a cell temperature of 675 °C, Ga was no longer detected in the films using AES. I - V measurements were also taken for digital and continuous films grown at various combinations of high and low Ga and Sc cell temperatures, but the breakdown fields were all <0.5 MV/cm.

IV. SUMMARY AND CONCLUSIONS

Initial experiments on low temperature MBE growth of $(\text{Sc}_2\text{O}_3)_x(\text{Ga}_2\text{O}_3)_{1-x}$ showed that Ga surface segregation is a major issue under most growth conditions. Higher growth temperatures would likely exacerbate this, suggesting that phase segregation will be a problem with most growth techniques. Even trying to make films of the type needed for feasible dielectrics for GaN-based devices was unsuccessful in the sense that poorer results were obtained compared to alloying with Gd. Previous results with $(\text{Gd}_2\text{O}_3)_x(\text{Ga}_2\text{O}_3)_{1-x}$ on GaAs revealed that the breakdown field strength increased as the films became richer in Gd.^{25,26} A film with a Gd concentration of 14% had a breakdown field of ~1.9 MV/cm, and the breakdown field increased to 2.5 MV/cm with an increase in the Gd concentration to 20%. However, the best results were obtained with a pure Gd_2O_3 film as it had an even higher breakdown field of 3.5 MV/cm. It appears that this same trend is present for $(\text{Sc}_2\text{O}_3)_x(\text{Ga}_2\text{O}_3)_{1-x}$ as films with increasing amounts of Sc exhibited higher breakdown fields with a pure Sc_2O_3 film having

the highest breakdown field (~2.70 MV/cm). It is believed that the incorporation of Ga into the films creates defects that diminish the insulating properties of the oxide.

Much more work is needed to optimize the growth of $(\text{Sc}_2\text{O}_3)_x(\text{Ga}_2\text{O}_3)_{1-x}$, but this initial work shows that other alloy systems may be more promising in terms of miscibility range and avoidance of surface segregation.

ACKNOWLEDGMENTS

The authors would like to thank the Research Service Center (RSC) staff at the University of Florida for their help in the fabrication and characterization of these materials. The work was performed as part of Interaction of Ionizing Radiation with Matter University Research Alliance (IIRM-URA), sponsored by the Department of the Defense, Defense Threat Reduction Agency under Award No. HDTRA1-20-2-0002. The content of the information does not necessarily reflect the position or the policy of the federal government, and no official endorsement should be inferred. The work was also supported by the NSF [No. DMR 1856662 (James Edgar)].

AUTHOR DECLARATIONS

Conflict of Interest

The authors have no conflicts to disclose.

DATA AVAILABILITY

The data that support the findings of this study are available within the article

REFERENCES

- 1E. Ahmadi and Y. Oshima, *J. Appl. Phys.* **126**, 160901 (2019).
- 2H. von Wenckstern, *Adv. Electron Mater.* **3**, 1600350 (2017).
- 3R. Wakabayashi, K. Yoshimatsu, M. Hattori, J.-S. Lee, O. Sakata, and A. Ohtomo, *Cryst. Growth Des.* **21**, 2844 (2021).
- 4S. J. Pearton, J. Yang, P. H. Cary, F. Ren, J. Kim, M. J. Tadjer, and M. A. Mastro, *Appl. Phys. Rev.* **5**, 011301 (2018).
- 5M. Xiao *et al.*, *IEEE Trans. Power Electron.* **36**, 8565 (2021).
- 6G. T. Dang, T. Yasuoka, Y. Tagashira, T. Tadokoro, W. Theiss, and T. Kawaharamura, *Appl. Phys. Lett.* **113**, 062102 (2018).
- 7A. F. M. Anhar Uddin Bhuiyan, Z. Feng, J. M. Johnson, Z. Chen, H.-L. Huang, J. Hwang, and H. Zhao, *Appl. Phys. Lett.* **115**, 120602 (2019).
- 8M. Dong, W. Zheng, C. Xu, R. Lin, D. Zhang, Z. Zhang, and F. Huang, *Adv. Opt. Mater.* **7**, 1801272 (2019).
- 9X. Liu, C. Sammarco, G. Zeng, D. Guo, W. Tang, and C.-K. Tan, *Appl. Phys. Lett.* **117**, 012104 (2020).
- 10M. Akiyama, K. Kano, and A. Teshigahara, *Appl. Phys. Lett.* **95**, 162107 (2009).
- 11M. A. Caro, S. Zhang, T. Riekkinen, M. Ylilammi, M. A. Moram, and O. Lopez-Acevedo, *J. Phys. C: Solid State* **27**, 245901 (2015).
- 12M. A. Moram and S. Zhang, *J. Mater. Chem. A* **2**, 6042 (2014).
- 13M. T. Hardy, B. P. Downey, N. Nepal, D. F. Storm, D. S. Katzer, and D. J. Meyer, *Appl. Phys. Lett.* **110**, 162104 (2017).
- 14C. Manz *et al.*, *Semicond. Sci. Technol.* **36**, 034003 (2021).
- 15M. T. Hardy, E. N. Jin, N. Nepal, D. S. Katzer, B. P. Downey, V. J. Gokhale, D. F. Storm, and D. J. Meyer, *Appl. Phys. Express* **13**, 065509 (2020).
- 16K. Frei *et al.*, *Jpn. J. Appl. Phys.* **58**, SC1045 (2019).
- 17J. Casamento, C. S. Chang, Y. T. Shao, J. Wright, D. A. Muller, H. Xing, and D. Jena, *Appl. Phys. Lett.* **117**, 112101 (2020).

- ¹⁸S. Fichter, N. Wolff, F. Lofink, I. Kienle, and B. Wagner, *J. Appl. Phys.* **125**, 114103 (2019).
- ¹⁹N. Zhu, B. Wang, K. Ma, X. Xue, and J. Su, *Appl. Phys. Lett.* **120**, 053503 (2022).
- ²⁰B. P. Gila, F. Ren, and C. R. Abernathy, *Mat. Sci. Eng. R* **44**, 151 (2004).
- ²¹C. Ostermaier, P. Lagger, M. Reiner, and D. Pogany, *Microelectron. Rel.* **82**, 62 (2018).
- ²²B. P. Gila, J. W. Johnson, K. N. Lee, V. Krishnamoorthy, C. R. Abernathy, F. Ren, and S. J. Pearton, *Electrochem. Soc. Proc.* **1**, 71 (2001).
- ²³B. P. Gila *et al.*, *Phys. Status Solidi A* **188**, 239 (2001).
- ²⁴M. Hlad, "Optimization stability of gate dielectrics on GaN," Ph.D. dissertation (University of Florida, 2007).
- ²⁵F. Ren *et al.*, *Solid State Electron.* **41**, 1751 (1997).
- ²⁶T. S. Lay, M. Hong, J. Kwo, J. P. Mannaerts, W. H. Hung, and D. J. Huang, *Solid State Electron.* **45**, 1679 (2001).
- ²⁷M. A. Berding, A. Sher, A. B. Chen, and R. Patrick, *Semicond. Sci. Technol.* **5**, S86 (1990).
- ²⁸J. Gersten and F. Smith, *The Physics and Chemistry of Materials* (Wiley, New York, 2001).
- ²⁹O. Dehaese, X. Wallart, and F. Mollot, *Appl. Phys. Lett.* **66**, 52 (1995).
- ³⁰K. Yamaguchi, T. Okada, and F. Hiwatashi, *Appl. Surf. Sci.* **117/118**, 700 (1997).
- ³¹S. Y. Karpov and Y. N. Makarov, *Thin Solid Films* **380**, 71 (2000).
- ³²J. Kim *et al.*, in *Materials Research Society Symposium Proceedings*, Boston, December 1985 (Pittsburgh, PA, 1985), Vol. 693, p. 699.
- ³³P. Waltereit, O. Brandt, K. H. Ploog, M. A. Tagliente, and L. Tapfer, *Phys. Rev. B* **66**, 165322 (2002).
- ³⁴M. Hong, Z. H. Lu, J. Kwo, A. R. Kortan, J. P. Mannaerts, J. J. Krajewski, K. C. Hsieh, L. J. Chou, and K. Y. Cheng, *Appl. Phys. Lett.* **76**, 312 (2000).
- ³⁵R. A. Stall, J. Zilko, V. Swaminathan, and N. Schumaker, *J. Vac. Sci. Technol. B* **3**, 524 (1985).
- ³⁶C. D. Wagner, A. V. Naumkin, A. Kraut-Vass, J. W. Allison, C. J. Powell, and J. R. Rumble, Jr., (2003), see <http://srdata.nist.gov/xps/> for NIST X-ray Photoelectron Spectroscopy Database, NIST Standard Reference Database 20, Version 3.4 (2007).